Available online at www.eccomasproceedia.org
Eccomas Proceedia COMPDYN (2023) 2229-2237

ECCOMAS
Proceedia

COMPDYN 2023
9th ECCOMAS Thematic Conference on
Computational Methods in Structural Dynamics and Earthquake Engineering
M. Papadrakakis, M. Fragiadakis (eds.)
Athens, Greece, 12-14 June 2023

DESIGN, TESTING AND MODELING OF A NOVEL FRICTION DAMPER WITH ENHANCED RESISTANCE TO REPEATED SEISMIC LOADS

V. Quaglini[1], E. Bruschi[1], C. Pettorruso[1], and M. Sartori[2]

[1] Politecnico di Milano
Piazza Leonardo da Vinci 32, 20133 Milan, Italy
e-mail: {virginio.quaglini, eleonora.bruschi, carlo.pettorruso}@polimi.it

[2] Freyssinet Products Italy SpA
Via dei Missaglia, 97, 20142 Milan, Italy
{mauro.sartori}@freyssinet.com

Abstract

The study presents the design, experimental characterization and modeling of a novel friction damper with enhanced resistance to repeated seismic loads. This device provides energy dissipation by the friction force triggered between a moving shaft and a lead core prestressed within a rigid steel chamber. As there are not mechanical parts that are subjected to cyclic stresses, there is no risk of fatigue and the damper is expected to resist to a virtually unlimited number of load cycles.

Two prototypes of the friction damper were tested according to the procedure established in the European standard EN 15129 for Displacement Dependent Devices, fulfilling the relevant requirements. The damper provides a stable response over repeated cycles, characterized by an essentially rectangular hysteresis loop with an equivalent viscous damping ratio ξ_{eff} of more than 55%. Moreover, the damper is characterized by a low sensitivity to the loading rate and by the ability to withstand multiple cycles of motion at the design earthquake displacement without deterioration of performance, providing maintenance-free operation in presence of repeated ground shakes.

A 3D finite element model of the friction damper is formulated in Abaqus and validated upon the results of the experimental tests. The model is then used in a parametric study to investigate the influence of the diameters of the shaft on the output force. The numerical data points are fitted by a simple model which can be used for designing the damper according to a specific quasi-static force.

Keywords: Friction Damper, Energy dissipation, Experiments, EN 15129.

ISSN:2623-3347
Peer-review under responsibility of the organizing committee of COMPDYN 2023.
doi: 10.7712/120123.10555.20303

1 INTRODUCTION

The PS-LED damper is a novel energy dissipation system recently presented in the literature by the Authors of this paper [1]-[8], to overcome most of the drawbacks associated to current energy dissipation devices. Indeed, hysteretic dampers are today the most popular devices used for the retrofitting of ordinary buildings, as demonstrated in numerous studies [9]-[18]. These dampers are normally installed within a brace; this configuration has a beneficial effect on the retrofitted structure since the braces provide an increase of structural stiffness that reduces the structural displacement, while the dampers dissipate a large part of the seismic energy, increasing the overall energy dissipation capacity of the structure and reducing the structural acceleration [19]-[21]. Nonetheless, the installation of the damped braces in existing structures requires an important amount of construction work, resulting in significant disturbance to the occupants and critical alterations to the building layout because of their excessive dimensions that ruin the aesthetic and architecture of the buildings [22].

In addition to that, conventional steel hysteretic dampers dissipate the seismic energy by yielding of a mild steel core and are typically affected from low-cycle fatigue; therefore, after a strong shock, they need to be replaced leaving the structure exposed to possible aftershocks [1], [4].

Other important drawbacks of these systems are associated to the increase of internal forces in beams and columns adjacent to the damped braces, due to the stiffening effect of the braces, which decreases the vibration period, hence generating an increase of vertical forces at foundation level and base shear [22]. This phenomenon requires further interventions to strengthen the columns and foundations of the main frame.

The novel damper dissipates the seismic energy through the friction mechanism generated between a lead core and a moving shaft; no mechanical parts get damaged, therefore the PS-LED is able to dissipate the seismic energy of multiple design earthquakes [2], [3]. The lead core inside the chamber is prestressed and it behaves like an incompressible fluid, subjected to a hydrostatic pressure regime. The axial strength of the damper can be easily adjusted by controlling the prestress of the core, allowing to achieve high specific strength (i.e., high force to volume ratio), thereby providing low dimensions which reduce the architectural invasiveness of the device [1]-[8].

The present contribution will follow this scheme: in Chapter 2, the PS-LED damper is presented, and the results of a parametric study conducted in Abaqus [23] are reported. Chapter 3 describes the two prototypes of the PS-LED that were tested and reports the adopted testing protocol. The results of the experimental campaign are presented and discussed in Chapter 4.

2 DESIGN AND MODELING THE PS-LED DAMPER

The PS-LED damper is characterized by a simple geometry made of four main parts, which are a rigid tube, a cap, a straight shaft and a working material made of lead, Figure 1. Tube, shaft and cap are made of structural steel, and the shaft is plated with hard chromium in order to minimize friction and wear during sliding through the bushing provided in the cap. The device is provided with spherical joints at the end of the shaft and of the main body in order to avoid transmission of bending moments (Figure 1).

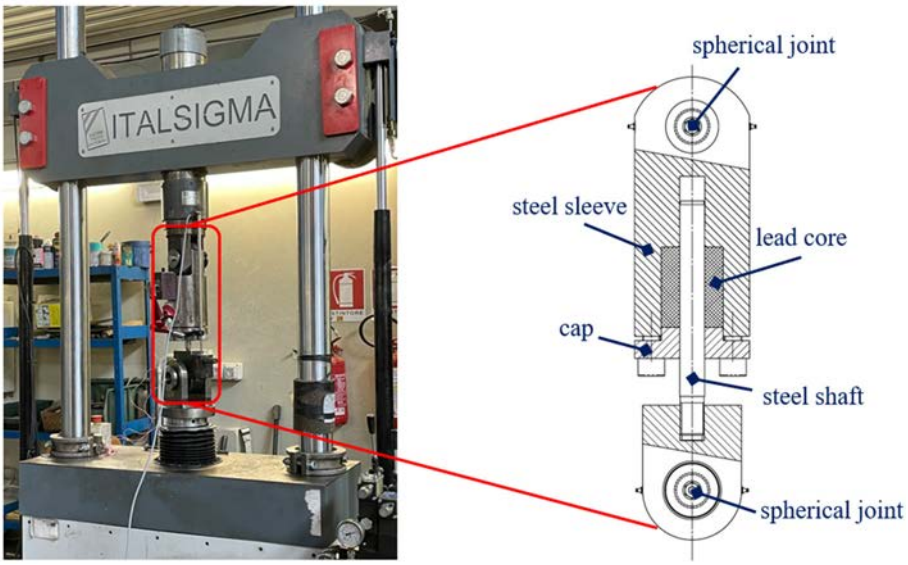

Figure 1: One of the prototypes on the testing machine and its section view with nomenclature of the PS-LED main parts.

The seismic energy is dissipated through the friction that is generated between the straight shaft and the lead. Since there are no mechanical parts that undergo inelastic deformations, this working mechanism guarantees that the device can resist to multiple shocks without any damage [2]-[4], [7], [8].

The lead core is prestressed by tightening the screws of the cap, in order to remove voids and clearances, resulting in a perfect fit to the tube and the shaft. The prestress allows to control the friction force of the device, guaranteeing a stable behavior without deterioration of stiffness and damping [1]-[8]. A numerical simulation was conducted in the general-purpose software Abaqus/CAE 6.14-2 [23] using 4-node bilinear axisymmetric elements type C4X4 and by modeling only half of the prototype thanks to its symmetry (Figure 2(a)). The parameters of the FE model are reported in Table 1. A fine mesh (3.3 mm maximum element size) was used to represent the volume of the lead, which was modeled as an elastic–almost perfectly plastic material, though a small hardening was introduced to avoid convergence issues. S450 steel material was assumed for the shaft, tube and cap. Hard contact was introduced at the interfaces between shaft and tube and between the shaft and cap, while hard contact in the normal direction and penalty friction formulation in the shear direction were assigned at the interfaces between the lead and shaft and between the lead and tube, where the relevant friction coefficients are $\mu_1 = 0.15$ and $\mu_2 = 0.30$, respectively [1]. The application of the prestress on the lead core was simulated by applying a force uniformly distributed on the cap. This force was increased until a fixed axial strain $\varepsilon = \Delta L/L$ of the lead bulk was achieved, where L is the initial height of the bulk and ΔL represents the change in this height. At this point, the force was held constant and dynamic implicit analysis was performed by imposing a cyclic displacement history to the shaft with a displacement amplitude of 20 mm. The analyses were performed considering different values of axial strain ε and different diameters of the shaft, specifically $D_s = 20$, 28 and 32.5 mm. The outer diameter of the lead core (Figure 1) was kept constant and equal to 70 mm. Figure 2(b) shows the results of the analyses, where it is evident that the axial force F_0 increases almost proportionally with ε until a certain threshold is reached, beyond which no further increase occurs. This limit coincides with the yielding of the lead and determines the maximum stress that can be induced in the material bulk, which is in turn proportional to the friction force. For this reason, the calculation of the force F_0 can be approximated as the product $\mu_1 \cdot p \cdot A$, where μ_1 is the coefficient of friction at the interface between the shaft and the

lead core, p is the contact stress at the interface and A is the area of the lateral surface of the shaft in contact with the lead core.

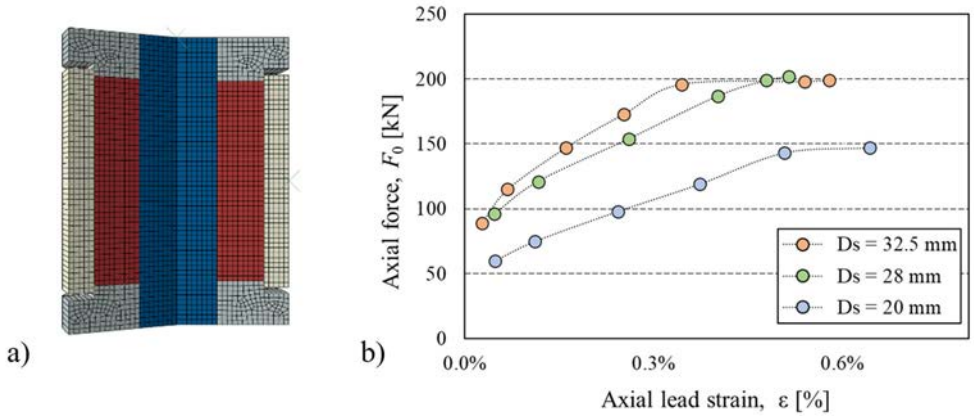

Figure 2: a) finite element model of the damper; b) axial force F_0 of the damper vs axial strain ε of lead core for different diameters of the shaft D_s.

Property	Unit	Steel		Lead	
Young's modulus (E)	GPa	210		16.4	
Poisson's ratio (υ)	–	0.33		0.44	
Density (ρ)	kg/mm^3	7.85×10^{-6}		8×10^{-6}	
Plastic behavior		Plastic strain	Stress [MPa]	Plastic strain	Stress [MPa]
		0	450	0	20.5
		0.2	500	0.001	21.5
				0.002	22.0
				0.1	22.5
				0.3	23.0

Table 1: Material properties of the FE model in Abaqus.

3 DESCRIPTION OF THE PROTOTYPES AND TESTING PROTOCOL

Two prototypes of the PS-LED were tested, whose geometry and design parameters (namely, design seismic displacements d_{bd} and design force N_d) are reported in Table 2.

Prototype	D_s [mm]	D_{cyl} [mm]	L_s [mm]	L_d [mm]	N_d [kN]	d_{bd} [mm]
#1	32.5	60	80	410	220	10
#2	20	70	70	385	50	15

D_s: diameter of the shaft; D_{cyl}: inner diameter of the tube wall; L_s: length of the lead core – shaft interface; L_d: axial length of the device; N_d: design axial force; d_{bd}: design seismic displacement in either direction

Table 2: Properties of the tested PS-LED prototypes.

The experimental campaign was conducted at the Materials Testing Laboratory of Politecnico di Milano, using a 500 kN servohydraulic testing machine (MTS Systems, Eden Prairie, MN), shown in Figure 1. The tests were performed by applying the protocol reported in Table 3. In particular, four different types of tests were performed, namely cyclic tests, ramp test, dynamic tests and survivability tests. Cyclic tests and ramp test are prescribed by the European Standard EN 15129 [24] for Displacement Dependent Devices (DDD). The cyclic tests consist in harmonic cycles of increasing amplitude at 25%, 50% and 100% of the design deflection d_{bd},

performing five cycles for each intermediate amplitude and ten cycles for the maximum amplitude (Table 3). The loading frequency was f_0 = 0.5 Hz for prototype 1, and 0.25 Hz for prototype 2. The ramp test requires to apply a monotonic ramp at 0.1 mm/s with increasing deformation up to the amplified displacement $\gamma_b\ \gamma_x\ d_{bd}$ where γ_b is the amplification factor equal to 1.1 and γ_x is the reliability factor equal to 1.2; in this study, the ramp test was applied considering two times the amplified displacement recommended in the standard [24] (Table 3).

In order to investigate the dependence of the behavior of the PS-LED on velocity, dynamic tests were performed by applying five harmonic cycles, each at d_{bd}, for different frequencies with 4 cycles at each frequency (Table 3).

Finally, three additional tests (named survivability tests in Table 3) were applied by imposing three sequences of ten cycles each of sinusoidal displacement at the design seismic displacement d_{bd}, with a dwell period of about 1 h between two consecutive sequences. These tests aimed at investigating the ability of the device to withstand multiple sequence of shocks.

Test	*d* [mm]	*f* [Hz]	*n° of cycles* [-]
cyclic	0.25 d_{bd}	f_0	5
	0.5 d_{bd}	f_0	5
	1.0 d_{bd}	f_0	10
ramp	$2 \cdot \gamma_x \cdot \gamma_b \cdot d_{bd}$	0.001	1
dynamic	1.0 d_{bd}	0.5 f_0	4
	1.0 d_{bd}	1.0 f_0	4
	1.0 d_{bd}	1.5 f_0	5
survivability	1.0 d_{bd}	f_0	10
	1.0 d_{bd}	f_0	10
	1.0 d_{bd}	f_0	10

Table 3: Testing protocol.

4 EXPERIMENTAL RESULTS

According to EN 15129 [24], the behavior of the PS-LED is evaluated on the basis of (i) the effective stiffness K_{eff} and (ii) the equivalent viscous damping ratio ξ_{eff}, which are determined according to the Equations (1) and (2)

$$K_{eff} = \frac{N}{d} \tag{1}$$

$$\xi_{eff} = \frac{2\ EDC}{\pi\ d\ N} \tag{2}$$

in which N is the force at the maximum deflection d in a cycle and EDC is the energy dissipated per cycle.

At each cycle, K_{eff} and ξ_{eff} are evaluated to check that their values remain almost constant during a sequence of same amplitude, with a variation of maximum ±10% with respect to the third cycle.

Figure 3 shows two experimental force-displacement hysteresis loops of the PS-LED prototypes. In both cases, it is evident the initial linear behavior that corresponds to the elastic deflection of the shaft, followed by a plastic branch characterized by a constant force independent of the accommodated displacement, which is symmetric in extension (N>0, shaft moving outwards) and in compression (N<0, shaft moving inwards). It is worth mentioning that the small curvature of the loop apparent at each motion reversal are due to a shallow dependence of the behavior on the velocity, though this dependency does not affect too much the overall response.

The idle displacement observed after the motion reversal and highlighted in Figure 3 by red arrows is due to the clearance of the spherical hinges.

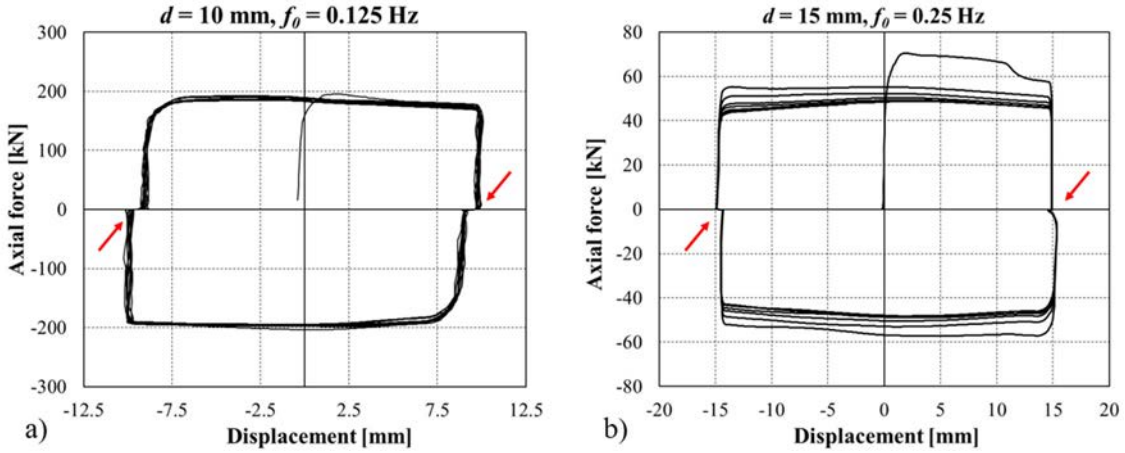

Figure 3: Examples of hysteresis loops of prototype 1 (a) and prototype 2 (b).

Both K_{eff} and ξ_{eff} fulfill the stability requirement of EN 15129 [24] showing maximum variations (with respect to the respective values evaluated at the third cycle, $K_{eff,3}$ and $\xi_{eff,3}$) of 9.9% and 2.4% for prototype 1, and of 7.6% and 0.9% for prototype 2, respectively. The average value of ξ_{eff} over 10 cycles performed at the design deflection is 0.55 for prototype 1 and 0.60 for prototype 2, really close to the maximum theoretical value of 0.63, confirming the excellent dissipation capacity of the PS-LED. After each sequence of tests, the prototype was left at ambient temperature for some time (45 min ÷ 90 min); this procedure is necessary to let the lead to recrystallize and recover its original properties.

Figure 4 shows the response of the prototype 1 to the survivability tests: the force-displacement plots relevant to the three sequences practically overlap to each other, demonstrating that the PS-LED is unaffected from low-cycle fatigue and suggesting that, in practical applications, the damper can sustain multiple design level earthquakes without needing to be replaced after a single event.

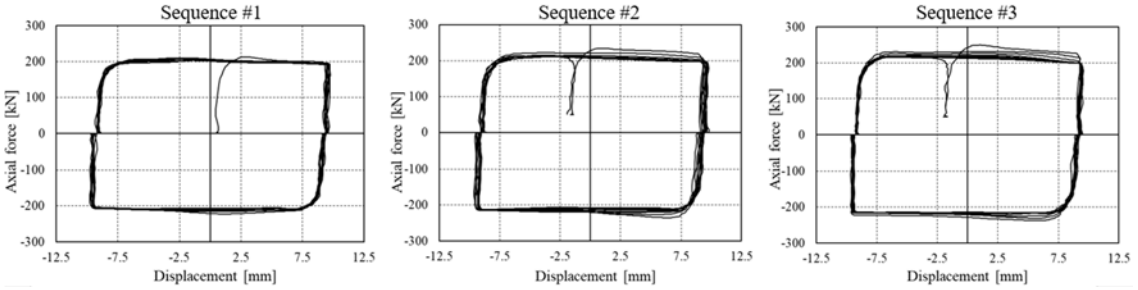

Figure 4: Response of the PS-LED (prototype 1) to the survivability tests [2].

Eventually, in the monotonic ramp test (Figure 5) the prototypes were able to sustain the amplified design deflection $2 \cdot \gamma_b \, \gamma_x \, d_{bd}$ and the force–deflection curves present a stable behavior, demonstrating the ability of the device to accommodate the prescribed displacement without any mechanical damage or deterioration of its stiffness.

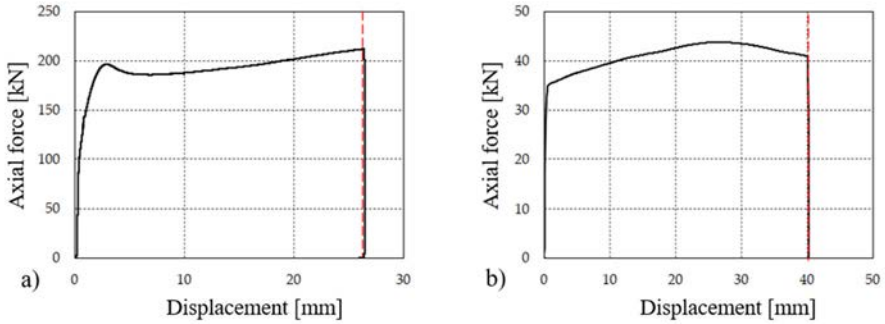

Figure 5: Ramp test to the amplified design deflection $2 \cdot \gamma_b \, \gamma_x \, d_{bd}$ for prototype 1 (a) and prototype 2 (b).

5 CONCLUSIONS

In this contribution, two prototypes of the PS-LED were experimentally investigated following the provisions for Displacement Dependent Devices of the European standard EN 15129 [24]. Both these dampers fulfilled the requirements of the norm [24], showing a stable and predictable mechanical response over a series of cycles. These devices are characterized by an essentially rigid–plastic behavior, with a constant axial force and an equivalent viscous damping ratio ξ_{eff} close to 60%.

The numerical analysis conducted in Abaqus [23] demonstrated that the output force of the PS-LED increases almost proportionally with the deformation of the core produced by prestressing the lead, until the yielding stress of the lead is reached, after which the force remains practically constant.

REFERENCES

[1] V. Quaglini, C. Pettorruso, E. Bruschi, Experimental and numerical assessment of prestressed lead extrusion dampers. *International Journal of Earthquake Engineering*, **XXXVIII**, 46-69, 2021.

[2] E. Bruschi, V. Quaglini, Assessment of a novel hysteretic friction damper for the seismic retrofit of reinforced concrete frame structures. *Structures*, **46**, 793-811, 2022. DOI: 10.1016/j.istruc.2022.10.113.

[3] E. Bruschi, L. Zoccolini, S. Cattaneo, V. Quaglini, Experimental characterization, modelling and numerical evaluation of a novel friction damper for the seismic upgrade of existing buildings. *Materials*, **16(5)**, 1933, 2023. https://doi.org/10.3390/ma16051933.

[4] V. Quaglini, C. Pettorruso, E. Bruschi, Design and experimental assessment of a prestressed lead damper with straight shaft for seismic protection of structures. *Geosciences*, **12**, 182, 2022. DOI: 10.3390/geosciences12050182.

[5] C. Pettorruso, E. Bruschi, V. Quaglini, Supplemental energy dissipation with prestressed Lead Extrusion Dampers (P-LED): Experiments and modeling. *8th ECCOMAS Thematic Conference on Computational Methods in Structural Dynamics and Earthquake Engineering*, Athens, Greece, 28–30 June 2021.

[6] V. Quaglini, E. Bruschi, C. Pettorruso, Design and experimental characterization of a novel Lead Damper for seismic protection of buildings. *3rd European Conference on Earthquake Engineering & Seismology*, Bucharest, Romania, 4-9 September 2022.

[7] V. Quaglini, E. Bruschi, C. Pettorruso, M. Sartori, Design and experimental assessment of a novel damper with high endurance to seismic loads. *Structural Integrity Procedia*, **44(C)**, 1451-1457, 2023. https://doi.org/10.1016/j.prostr.2023.01.186.

[8] E. Bruschi, V. Quaglini, Numerical investigation on the seismic performance of a RC framed building equipped with a novel Prestressed LEad Damper with Straight Shaft. *Structural Integrity Procedia*, **44(C)**, 1443-1450, 2023. https://doi.org/10.1016/j.prostr.2023.01.185.

[9] F. Aliakbari, S. Garivani, A.A. Aghakouchak., An energy based method for seismic design of frame structures equipped with metallic yielding dampers considering uniform inter-story drift concept. *Engineering Structures*, **205**, 110114, 2020. DOI:10.1016/j.engstruct.2019.110114.

[10] E. Gandelli, A. Taras, J. Disti, V. Quaglini, Seismic retrofit of hospitals by means of hysteretic braces: influence on acceleration-sensitive non-structural components. *Frontiers in Built Environment*, **5**, 100, 2019. DOI: 10.3389/fbuil.2019.00100.

[11] E. Gandelli, S. Chernyshov, J. Distl, P. Dubini, F. Weberd, A. Taras, A. Novel adaptive hysteretic damper for enhanced seismic protection of braced buildings. *Soil Dynamics and Earthquake Engineering*, **141**, 106522, 2021. DOI: 10.1016/j.soildyn.2020.106522.

[12] E. Bruschi, V. Quaglini, P.M. Calvi, A simplified design procedure for seismic upgrade of frame structures equipped with hysteretic dampers. *Engineering Structures*, **251**, e113504, 2021. DOI: 10.1016/j.engstruct.2021.113504.

[13] V. Quaglini, E. Bruschi, C. Pettorruso, Dimensionamento di dispositivi dissipativi per la riabilitazione sismica di strutture intelaiate. *Structural*, **e237**, 2021. DOI: 10.12917/STRU237.25.

[14] E. Bruschi, V. Quaglini, P.M. Calvi, A simplified design procedure to improve the seismic performance of RC framed buildings with hysteretic damped braces. *New Metropolitan Perspectives 2022 - 5th International Symposium "Post COVID Dynamics: Green and Digital Transition, between Metropolitan and Return to Villages' Perspectives"*, Reggio Calabria, Italy, 25-27 May 2022, Volume 482 LNNS, pp. 2173 – 2182, ISBN: 978-3-031-06825-6.

[15] E. Bruschi, V. Quaglini, L. Zoccolini, Control of the seismic response of steel-framed buildings by using supplementary energy dissipation devices, *Applied Sciences*, **13(4)**, 2063, 2023. DOI: 10.3390/app13042063.

[16] V. Quaglini, E. Bruschi, Controllo passivo mediante controventi dissipativi. Principi generali, requisiti normativi ed evoluzione dei principali dispositivi a comportamento dipendente dallo spostamento. *Structural*, **240**, 09. 2022. DOI: 10.12917/STRU240.09.

[17] S. Garivani, S.S. Askariani, A.A. Aghakouchak, Seismic design of structures with yielding dampers based on drift demands. *Structures*, **28**, 1885–1899, 2020. DOI: 10.1016/j.istruc.2020.10.019.

[18] M.Z. Golmoghany, S.M. Zahrai, Improving seismic behavior using a hybrid control system of friction damper and vertical shear panel in series. *Structures*, **31**, 369–379, 2021. DOI: 10.1016/j.istruc.2021.02.007.

[19] F. Freddi, J. Ghosh, N. Kotoky, M. Raghunandan, Device uncertainty propagation in low-ductility RC frames retrofitted with BRBs for seismic risk mitigation. *Earthquake Engineering and Structural Dynamics*, **50**, 2488-2509, 2021. DOI: 10.1002/eqe.3456.

[20] F. Bartera, R. Giacchetti, Steel dissipating braces for upgrading existing building frames. *Journal of Constructional Steel Research*, **60**, 751-769, 2004. DOI: 10.1016/S0143-974X(03)00141-X.

[21] F. Yang, G. Wang, M. Li, Evaluation of the seismic retrofitting of mainshock-damaged reinforced concrete frame structure using steel braces with soft steel dampers. *Applied Sciences*, **11**, 841, 2021. DOI: 10.3390/app11020841.

[22] J.E. Martínez-Rueda, On the evolution of energy dissipation devices for seismic design. *Earthquake Spectra*, **18(2)**, 309-346, 2002. DOI: 10.1193/1.1494434.

[23] Dassault Systemes Simulia Corp. Abaqus/CAE user's guide, Providence, 2017.

[24] CEN (European Committee for Standardization). European Committee for Standardization (2009). EN 15129. Anti-seismic devices. Brussels.